RSC Sustainability

ROYAL SOCIETY OF CHEMISTRY

PAPER

View Article Online
View Journal | View Issue



Cite this: *RSC Sustainability*, 2023, **1**, 270

# Highly efficient lithium-ion battery cathode material recycling using deep eutectic solvent based nanofluids†

Changhui Liu, *[a] Yuqi Cao,[a] Wenjie Sun,[a] Tianjian Zhang,[c] Hongqu Wu,[e] Qingyi Liu,[a] Zhonghao Rao *[b] and Yanlong Gu *[cd]

Waste battery materials are precious resources that can be recycled under certain specific conditions. Traditional recycling methods require high energy consumption, have low efficiency, and lead to serious pollution. With the aim of developing a mild and efficient approach to recycle spent cathode materials of lithium-ion batteries (LIBs), nanoparticles dispersed in deep eutectic solvents (DESs), herein referred to as nanofluids, for the first time, were utilized as a medium for recycling LIBs. 100% liberation efficiency was achieved under mild conditions thanks to the collaboration of DESs and nanoadditives, in which DESs worked as a medium for dispersing of cathode materials and nanoadditives enable an enhancement of heat and mass transfer of the solvent system. Notably, though the main aim of this work is the liberation of the cathode active material from spent LIBs, it is shown that the presence of nano-additives in DESs could double the metal leaching efficiency in comparison to that of pure DESs. A mechanistic study of static thermal properties and dynamic observation of nanofluids demonstrated that the liberation rate could be enhanced by 15% with a 0.8% thermal conductivity ($k$) enhancement when boron nitride (BN) was employed as a nanoadditive. Additionally, simulation of the recycling process *via* a computational fluid dynamics (CFD) method indicated that mass transfer plays a key role in enhancing the recycling rate of LIB materials. Moreover, DESs could be used at least five times without affecting their recycling activity. In view of the low energy consumption, low toxicity, recyclability, and simplicity of the experimental procedure described herein, it offers a promising approach for the recycling of LIB cathode materials at an industrial scale.

Received 14th September 2022
Accepted 7th December 2022

DOI: 10.1039/d2su00047d

rsc.li/rscsus



## Sustainability spotlight

It is well-known that resources of lithium-ion batteries are nearing exhaustion because of the widespread development and use of electric vehicles. Waste battery materials are precious resources that can be recycled under certain specific conditions. Traditional recycling methods which mainly rely on pyrometallurgy and hydrometallurgy, require high energy consumption, have low efficiency, and lead to serious pollution. Herein, deep eutectic solvent based nanofluids, were utilized for the first time as a medium for recycling lithium-ion batteries. Realistic spent ternary lithium-ion battery cathodes were used as starting materials and afforded 100% liberation efficiency under mild conditions. A twofold leaching rate compared with pristine deep eutectic solvents could be reached. Moreover, deep eutectic solvents could be used at least five times without affecting their recycling activity.

## Introduction

As an important part of the new energy transportation tools, the popularity of electric vehicles has been rapidly increasing among consumers since they entered the market owing to their environmental friendliness, low noise, and high efficiency.[1–3] The global sales of electric vehicles will reach 140 million units by 2030; however, as the most frequently used batteries in electric vehicles, the number of waste lithium-ion batteries (LIBs) is expected to reach over 11 million tons by 2030.[4] In stark contrast to the rapidly increasing amount of LIBs being wasted, the amount of this material being recycled is less than 5% of the

[a]*School of Low-carbon Energy and Power Engineering, China University of Mining and Technology, Xuzhou, Jiangsu 221116, China. E-mail: liuch915@cumt.edu.com*

[b]*School of Energy and Environmental Engineering, Hebei University of Technology, Tianjin 300401, China. E-mail: raozhonghao@cumt.edu.cn*

[c]*School of Chemistry and Chemical Engineering, Huazhong University of Science and Technology, Wuhan, Hubei 430074, China. E-mail: klgyl@hust.edu.cn*

[d]*School of Chemistry and Chemical Engineering, The Key Laboratory for Green Processing of Chemical Engineering of Xinjiang Bingtuan, Shihezi University, Shihezi, Xinjiang 832003, China*

[e]*Key Laboratory of Microbial Pesticides, Ministry of Agriculture and Rural Affairs, Hubei Biopesticide Engineering Research Centre, Hubei Academy of Agricultural Sciences, Wuhan 430064, China*

† Electronic supplementary information (ESI) available. See DOI: https://doi.org/10.1039/d2su00047d

total amount used.[5,6] The accumulation of spent LIBs is harmful to the environment and human health.

Direct disposal of spent but unrecycled LIBs is a terrible waste of precious raw materials.[5,7] For example, cobalt constitutes up to 15 wt% of NMC111 battery materials and plays a dominant role in adjusting the charging performance of these materials. Furthermore, the cost of cobalt is relatively high, and it is mainly sourced from poor areas riddled with conflict (about 7.4 million tons of estimated reserves in the world).[6,8–10] Nickel rich cathode based batteries emerge as a hot research topic thanks to their wide use in high energy density electric vehicles which has led to the urgent rational reuse of this precious metal element.[11,12] Therefore, spent LIBs must be recycled to reduce the costs of LIBs and alleviate the constraints on this mineral resource.[13,14] LIBs are mostly composed of a battery shell, a cathode, an anode, an organic electrolyte, a membrane separator, and a battery case.[15–18] A commonly used LIB cathode is composed of aluminum (Al) foil, an organic binder, and a cathode material. By comparison, the anode largely consists of copper foil, an organic binder, and anode materials.[19–21] Raw metal species comprise the cathode; thus, the main concern is the recycling of raw metal elements in cathode materials.[22,23]

Several studies focused on the recycling and reuse of valuable metals in cathode materials. The recycling of the cathode mostly relies on three approaches, namely, pyrometallurgy, hydrometallurgy, and the novel solvent-leaching method. Pyrometallurgy occupies a superior position in various industries despite its high energy input owing to extremely high temperatures (up to 1400 °C). However, in pyrometallurgy, the off-gassing of harmful fumes and the subsequent scrubbing of the facility of recycling systems pose a heavy burden to LIB manufacturing. Additionally, the harsh reaction conditions and harmful gas emissions of this process demand strict safety precautions.[24,25] More importantly, the mixed slag obtained by pyrometallurgy makes the full recycling of metals impossible, especially under extremely high temperature conditions.[26] In comparison to pyrometallurgy, hydrometallurgy is recognized as the most efficient way for recycling LIB cathodes owing to the high leaching rate of the desired metal elements with a relatively high purity.[27,28] However, this technique leads to secondary pollution owing to the use of strong acidic reagents, such as hydrochloric acid, sulfuric acid, and nitric acid, which pose a safety risk to both the environment and human health (Fig. 1a).[29–31] Many researchers have attempted to develop new


Fig. 1 Schematic illustration of LIB cathode material recycling: (a) traditionally used and chemical solvent dissolution methods for metal recycling in spent LIBs; (b) comparison and nanofluid-aided cathode material liberation process.

solvent alternatives that have the advantages of hydrometallurgy and avoid the use of hazardous acidic reagents.[30] In this study, we refer to these protocols for cathode recycling as novel solvent-leaching methods. For example, some organic acidic solvents, such as malic acid and oxalic acid, can reportedly leach the metal element. However, they require the addition of a reduction reagent or extremely high temperatures, both of which severely hinder their widespread use, especially because of their poor thermal or chemical stability.[28,32] Deep eutectic solvents (DESs) have emerged as novel ionic liquid alternatives because of their good chemical stability, low saturated pressure, and wide liquid range.[33–35] Owing to hydrogen bond association between the hydrogen bond donor and acceptor, DESs have been proved to possess a unique ability to digest common metal oxides and recovery of valuable metal species from spent LIBs. For example, Tran *et al.*[36] pioneered the use of sustainable ethylene glycol (EG)/choline chloride (ChCl) DESs with low toxicity for the leaching of $LiCoO_2$ below 220 °C. Wang *et al.*[37] used DESs composed of urea/ChCl to recover $LiCoO_2$ at a lower temperature of 180 °C. Guo *et al.*[38] designed a novel DES consisting of EG and sulfosalicylic acid dihydrate (SAD) for efficient leaching of valuable metals from cathode active materials. The authors described the mechanism in which a reduction and coordination process were involved. Kinetics of the metal leaching process was also discussed. In the meantime, Guo *et al.*[39] developed a bifunctional DES based on EG and oxalic acid dihydrate (OAD) for selective extraction of valuable metals from spent LIBs. They also demonstrated a novel strategy for selective extraction of Ni, Co, and Mn respectively from the spent $LiNi_xCo_yMn_{1-x-y}O_2$ cathode through the regulation of the coordination environment of DESs.[40] Schiavi[41] reported a protocol for selective recovery of cobalt in which an extraction of 90% for cobalt and only 10% for nickel were achieved from cathode materials of LIBs by using EG/ChCl DESs. Hartley *et al.*[42] found that nickel oxide can be efficiently separated from cobalt and manganese oxides using an oxalic acid-based DES. Compared with pyrometallurgy and hydrometallurgy, novel solvent-leaching methods are clearly better as they do not produce extra waste and they use environmentally benign solvents. More importantly, they are more sustainable than pyrometallurgy or hydrometallurgy because the starting materials they use can be either recycled or biodegraded.[43]

Although advances have been made in solvent-leaching methods, some inherent problems still cannot be ignored, the most predominant of which is the use of commercially available $LiCoO_2$ rather than pristine spent LIBs to study recycle efficiency. Moreover, they still require a high temperature to achieve a relatively high metal leaching rate. Liberating cathode active materials from waste batteries is a kind of primary work which heavily affects the downstream recycle or recovery work. Conventional treatment methods largely rely only on mechanical crushing, which would lead to a poor recycle efficiency as cathode species still adhere to the aluminum foil.[44] Recently, Abbott *et al.* developed a rapid and simple method for removing the active material from composite electrodes using high powered ultrasound in a continuous flow process.[45] Chemical dissolution has also been proved to be a feasible recycling method. However, the high cost and environmentally harmful characteristics of this method hamper its wide application. Moreover, the specific devices used in this method and its high temperature requirement make it impractical in all occasions.[46,47] Dissolution of organic binders is a promising idea for the complete separation of cathode materials from aluminum foil. The organic layer on the surface of cathode particles can negatively affect the efficiency of subsequent reactions, thereby reducing the leaching efficiency of valuable metals. Moreover, the residual organic binder can contaminate the chemical reagents and reduce the purity of the recovered product. More importantly, though a series of promising approaches relying on DESs for recycling valuable metals from LIBs have been unveiled, we found that, so far, no reports regarding the study on heat and mass transfer characteristics in the liberation process exist. On the other hand, a milder and neutral condition enabling highly efficient cathode material liberation is also highly desirable. By contrast, owing to the advantageous heat and mass transfer properties of nanofluids, they have emerged as promising materials, and their use in thermal management and energy storage and conversion has been studied.[48,49] Nanofluids have been recently proved to be applicable as electrolytes, and they are superior to pristine base solutions.[50] And the release of cathode materials in spent LIBs is also a heat and mass transfer process in which the binder should be dissolved first. In light of these reported results, we explored whether nanofluids can be used as a medium to liberate precious metals from spent LIBs by using DES-based solvents. Herein, we prepared several nanofluids based on EG/ChCl DESs, and then subjected them to metal species recycling in LIBs. This study was the first to utilize nanofluids to recover spent LIBs. Owing to the enhanced heat and mass transfer effects, 100% liberation efficiency could be achieved at a relatively low temperature (Fig. 1b). Moreover, the DESs could be recycled at least five times without efficiency loss and disruption of the molecular structure. The underlying mechanism was studied by determining the exact thermophysical properties of the nanofluids and *via* computational fluid dynamics (CFD) simulation. Moreover, the participation of the nanofluids not only helped in liberating cathode materials from the spent LIBs but also enhanced the leaching efficiency of precious metals, in which the leaching rates of nickel, cobalt, and manganese could be doubled at 120 °C and 140 °C.

## Experimental section

### Materials information

Ethylene glycol (EG, AR, general-reagent) used in the experiment was purchased from Shanghai General Reagent, choline chloride (ChCl, 99%, Adamas-beta) was purchased from Sinopharm Chemical Reagent Company, nano silica (15 ± 5 nm, purity 99.5%), nano silicon carbide (50 nm), nano carbon black (100 nm, purity 99.5%), nano boron nitride (with diameter <200 nm, 500 nm, 1–2 μm and 5–10 μm, 99.9% metal basis), and dimethyl carbonate (DMC) were purchased from Shanghai Maclean Biochemical Technology Co., Ltd, nano graphene oxide (RGO) was prepared by the Hummers' method according

 

to a reported method,[51] and nano-graphene (surface area 500 $m^2\ g^{-1}$) was purchased from TCI (Shanghai) Chemical Industry Development Co., Ltd. The soft-pack battery used in the experiment (the cathode active material is NMC111) was manually disassembled after being fully discharged (data used in this paper were obtained by using soft-pack LIBs from the same supplier to keep a consistent variant; the process was repeated five times to determine the stable data). Deionized water is made using a laboratory ultrapure water filter (China, Nanjing Qianyan Instrument Equipment Co., Ltd, RO).

### Nanofluid preparation process

The reaction was carried out in a 100 ml round bottom flask with a magnetic stirrer. EG/ChCl DES (30 ml) was mixed with six nanoparticles (depending on the mass fraction of nanofillers) and then the mixture was heated to 100 °C and stirred for 2 hours. After the reaction, the mixture was cooled to room temperature. Subsequently, the solution was sonicated (53 kHz) for 2 h to obtain the final nanofluid.

### Experimental methods

EG/ChCl DESs with different molar ratios were prepared by a heating and magnetic stirring process. Nanofluids were prepared by a sequential dispersing, magnetic stirring and sonification process. For the liberation process, cathode materials were first cut into a size of 1 $cm^2$ with scissors. Unless otherwise noted, the liberation process was carried out in an oil bath at 600rpm at a specific reaction temperature. Liberated cathode materials were collected by vacuum filtration and dried. Leaching efficiency was calculated based on the ICP analysis (detailed calculation procedure can be found in the ESI†).

### Liberation rate of spent LIBs

The liberation rate is calculated according to eqn (1):

$$\eta = \frac{M - M_1}{m} \times 100\% \quad (1)$$

where $\eta$ is the liberation rate; $M$ represents the mass of the pristine cathode added in the experiment; $M_1$ is assigned to the mass of the cathode after reaction and drying; $m$ is the total mass of isolatable active species in pristine cathode materials.

### A typical recycling experimental procedure

DES was prepared with ChCl : EG = 3 : 1 (molar ratio) after stirring in an oil bath for 3 h at 100 °C. In the first round, nanofluids were prepared before LIB recycling. 30 ml DES was added to a round bottom flask and boron nitride (BN) nanoparticles (0.2 wt%) were then added; the nanofluids were obtained after stirring in a 100 °C oil bath for 1 h and being sonicated in a 40 kHz sonicator for 1 h. After this, the spent cathode material sheet (1.0 g) was added and the reaction was carried out in an oil bath at 100 °C and 600 rpm for 20 h. Afterwards, DES was recovered with filtration and made into nanofluid with the addition of a determined amount of BN (0.2 wt%) before being used in another cathode material recycle run. Cathode materials were collected and washed with deionized water. The recovered DES was used in the downstream cathode material recycling after being made into nanofluids by the same method as the first round.

### Characterization

The thermal conductivity of the nanofluid is measured using a Xiatech TC3000L liquid thermal conductivity analyzer in the temperature range of 30–60 °C. The viscosity of the nanofluid was measured with a digital rotational viscometer (LVDV-2T), Shanghai Fangrui Instrument Co., Ltd, China in the temperature range of 30–60 °C. Infrared photos were taken using an infrared thermal imager (FLIR C2, Filial).

### Computational fluid dynamics modeling method

Ansys Fluent 2020 software was used to numerically simulate the magnetic stirrer and its flow transfer characteristics. The magnetic stirrer was simplified to a commonly used stirring chest model. It consists of two major parts, the external fluid and the rotation domain (Fig. 4a).[52] And spaceclaim 2020 was used for geometry and boundary conditions; Ansys Fluent meshing 2020 was used for the mesh. The computational domain is divided into a rotational domain and stationary domain, and encryption is performed at each boundary. The geometry and mesh partitioning are shown in Fig. 4b.

The rotor rotates at a high speed in the rotational domain and exchanges velocity and LIB components with the stationary domain through the interface. The main concern is the stirring mass transfer of lithium-ion battery cathode particles in a DES based nanofluid. In the numerical calculations the two parameters are the velocity gradient of the solid–liquid system and lithium-ion battery cathode particle content distribution. Therefore, the Eulerian multiphase flow model and the multi-reference frame (MRF) method were used for the simulation, assuming a constant diameter of 11.2 μm for the lithium-ion battery cathode particles. And the lithium-ion battery cathode particles are uniformly distributed in the lower 1/5 of the stirrer according to the experimental specifics. The experimental parameters and initialization settings are shown in Table S2 and S3,† and the kinetic diagram of the component transport of LIBs with stirring is shown in the ESI.† The discretization equations were solved using the SIMPLE separation algorithm with default values for the model constants. The second-order upwind momentum method and the second-order implicit transient formulation were used. The appropriate time step is set to 0.01 s. The convergence of the calculations is evaluated by detecting whether the residuals of the iterations are less than $10^{-3}$.

## Results and discussion

### Optimization of experimental conditions

The liberation of LIBs was optimized. Cathode materials, which were dismantled from spent ternary LIBs by cutting them with scissors, were directly used. One of the components of DESs, namely, EG, was initially used as a liberation solvent. Pristine EG achieved a 38.29% liberation rate after heating at 100 °C for 24 h (Fig. 2a). EG/ChCl DESs with different blending ratios were

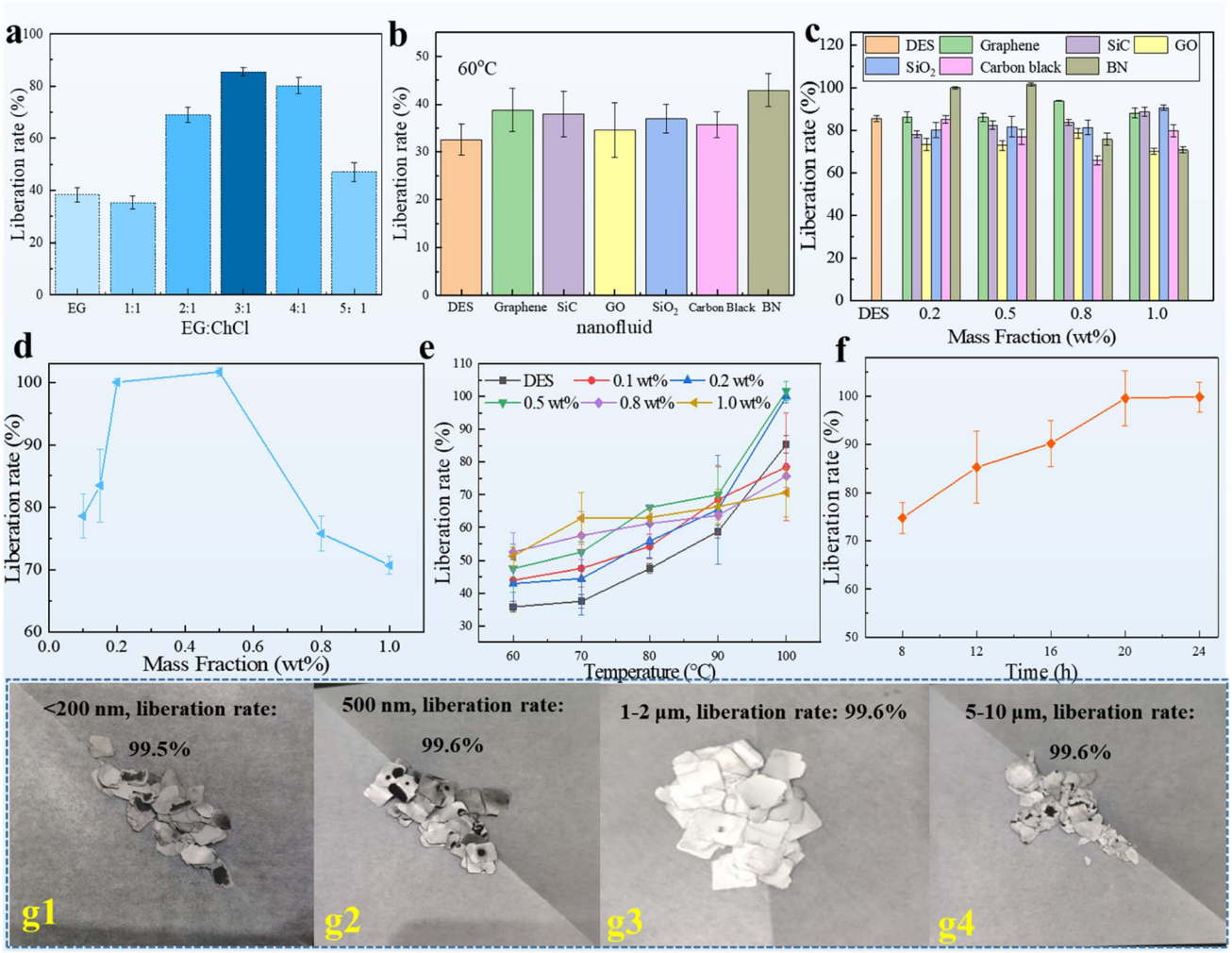


Fig. 2 Recycle rate of cathode materials from LIBs in the presence of DESs and the corresponding nanofluids. Liberation rates in (a) EG and DESs. (b) DES and six DES-based nanofluids (at 60 °C and 0.2 wt%). (c) Six DES-based nanofluids. The liberation rate in BN-filled nanofluids as functions of (d) mass fractions of BN. (e) Reaction temperature and (f) reaction time (unless otherwise noted, the liberation condition is as follows: liberation at 100 °C for 20 h). The liberation rate as a function of diameter of BN: (g1) <200 nm, (g2) 500 nm, (g3) 1–2 μm, and (g4) 5–10 μm.

then studied. The addition of ChCl into EG resulted in the formation of a eutectic solvent mediated by hydrogen bonding between each other, thereby changing the thermophysical properties and chemical characteristics, especially dissolvability.[53] Indeed, the participation of ChCl, which mainly acted as a hydrogen bond acceptor, achieved a liberation efficiency enhancement of 84.5% when the molar ratio between EG and ChCl was 3 : 1. The other ratios between these two components were also tested. However, their liberation ratios were less efficient than those of 3 : 1. This result indirectly suggested that the optimized ratio between EG and ChCl might lie within the range of 2 : 1–4 : 1 because of the existence of a rational ratio in the hydrogen bond donor and acceptor. Owing to the relatively low temperature requirement and simple work-up of this procedure, EG/ChCl deep eutectic solvent (DES) could be a promising liberation alternative for recovering LIB cathode materials. However, this result was considerably less satisfactory than we expected. In a previous study, we studied several DES-based nanofluids and observed an interesting phenomenon. In almost all cases, we found that heat and mass transfer performance can be improved compared with the base solvent.[54–56] The liberation of cathode materials in spent LIBs is a heat and mass transfer process in which the binder, that is, PVDF, should be first dissolved or degraded in the solvent atmosphere.[35,57] The cathode materials are then liberated from the aluminum foil. Diffusion of solute molecules is a premise of dissolution in which external heat is beneficial for the dissolution speed and degree. The application of external heat accelerates the speed and enhances the degree of dissolution.[54] Turbulence is another important factor that determines dissolution efficiency.[58] These main factors are consistent with the positive functions of nanofluids, namely, heat and mass transfer enhancement. To further improve the liberation efficiency, we first dispersed several nanoparticles into EG/ChCl DES-based solvents to form nanofluids and then used them to recover cathode materials from LIBs. In this study, six different nanoparticles, namely, graphene, $SiO_2$, graphene oxide (GO), SiC, carbon black, and BN, were studied. The liberation experiment was first carried out at

60 °C; it is found that BN filled nanofluids clearly stood out which afforded the best liberation ratio among the tested nanoparticles (Fig. 2b). Furthermore, adding just a 0.2% mass fraction of BN achieved 100% liberation at an elevated reaction temperature (Fig. 2c). Moreover, not all the nanoparticles studied herein had a positive effect on the liberation of cathode materials from LIBs. For example, the addition of GO decreased the liberation rate. Graphene had a liberation efficiency comparable to that of BN at a relatively high concentration of the nanoparticles. The most suitable nanoparticle was determined, and then its parameters were considered. The results showed that excessive or scarce application of BN did not attain a promising liberation yield. The optimized mass fraction range of the nanoparticles was 0.2–0.5%, within which a 100% liberation rate could be obtained (Fig. 2d). Thus, 0.2 wt% was chosen for further study because it was economical and required facile operation. A lower temperature was studied with respect to various mass fractions of BN (Fig. 2e). Temperature also played an important role in liberating cathode materials from spent LIBs as the liberation rate decreased to 50% at 60 °C. Another interesting phenomenon was observed. As more BN was added, the liberation rate was better at a relatively low experimental temperature (60 °C and 70 °C). However, this trend gradually changed as the liberation temperature was increased. The reaction time was also considered (Fig. 2f). The liberation rate remained steady after stirring at 100 °C for 20 h. Thus, further prolonging the reaction time made the data more stable. Therefore, the final reaction time was determined to be 24 h. Finally, the use of 0.2 wt% BN as the nanoparticle with a stirring time of 24 h at 100 °C was determined to be the optimal condition for liberating cathode materials. In addition, the diameter of BN was considered, as is seen in Fig. g1–4; the diameter of BN has a slight impact on the liberation rate; BN with a diameter of 1–2 μm was chosen in downstream experiments in terms of cost issues.

## Mechanistic study of the thermophysical properties of nanofluids

The mechanism underlying the distinct liberation rate of cathode materials from spent LIBs was investigated. The different thermophysical properties of various nanoparticles would lead to different liberation rates. Thus, the thermophysical properties of the nanofluids were considered. Two of the most important thermophysical properties, namely, thermal conductivity ($k$) and viscosity, are associated with heat and mass transfer respectively. The addition of nanoparticles increased $k$ (Fig. 3a). $k$ of each sample was recorded seven times to prevent errors in the testing process. Histograms of $k$ with different mass concentrations were plotted (Fig. 3b and c). Regardless of the mass concentration and test temperature, $k$ of BN-filled nanofluids was slightly different from that of the other five types of nanofluids. This result was reasonable because only a tiny amount of the nanoparticles was added. The viscosities of the different nanofluids were then tested at different test temperatures. The addition of nanoparticles inevitably increased viscosity (Fig. 3d). The Viscosity of BN-filled nanofluids was at the lower level of the six types of nanoparticle-filled nanofluids, especially at a lower test temperature. Therefore, the static thermophysical properties had a limited impact on the liberation rate of LIB cathode materials. Nevertheless, some indirect information could be obtained from the relatively high $k$ and low viscosity: an enhanced $k$ and a low viscosity were beneficial for the liberation of cathode materials. However, these pieces of information were insufficient to explain why the BN nanofluids displayed a superior performance in cathode material liberation. A dynamic experimental platform mimicking the actual experiment conditions was set up (Fig. S2†). The temperature of the solvent was recorded using an infrared camera (Fig. 3e). The response to temperature was more drastic in the case of BN- and graphene-filled nanofluids, especially in the first 10 s at a heating temperature of 80 °C. More importantly, the temperature of the BN- and graphene-filled nanofluids tended to remain steady in 60 s, whereas that of the other nanoparticle-filled nanofluids required at least 80 s to stabilize. Additionally, the temperature response of nanofluids at a 200 °C heating temperature displayed a similar phenomenon to that observed at 80 °C in which the BN nanofluid achieves a stabilization temperature of around 90 °C after being heated for 60 s, while the other nanofluids require a longer time. This experiment provided evidence that the BN- and graphene-filled nanofluids had a better liberation rate than the other nanofluids in terms of heat transfer characteristics.

## Mechanistic study *via* CFD simulation

Investigation into static thermophysical properties and experiments on dynamic heat transfer provided some useful information to understand the reason responsible for the superiority of BN-filled DES-based nanofluids. However, direct evidence was still lacking, especially on the mechanism of mass transfer. The effect of mass transfer on cathode material recycling was clarified *via* CFD simulation. It should be noted that parameters used in this simulation were tested at 60 °C, a temperature closest to 100 °C, owing to the temperature limitation of thermal conductivity and viscosity measurement facilities. The detailed parameters and the simulation process can be found in the ESI (Fig. S3 and S4†). The magnetic stirrer and the reaction flask were treated as a commonly used stirrer with two blades and a cylindrical tank respectively (Fig. 4a and b). The specific experimental conditions for the simulation of mass transfer were fixed at 60 °C and 600 rpm, consistent with the actual conditions. The mass transfer performance of each DES-based nanofluid was evaluated by determining the velocity gradient and volume fraction of the cathode materials in LIBs. Cloud images of velocity on the $x$-axis and at the center of the rotational domain were plotted and are shown in Fig. 4c and d, respectively. The DES-based nanofluids had a clear enhancement in velocity compared with the pristine base solvent owing to their enhanced mass transfer properties. Notably, the BN-filled nanofluids had the quickest velocity response as shown in the $x$-axis cloud images (Fig. 4c). Moreover, the velocity of the solution in other profiles was determined using histograms (Fig. 5a and b). The results agreed well with the cloud images:

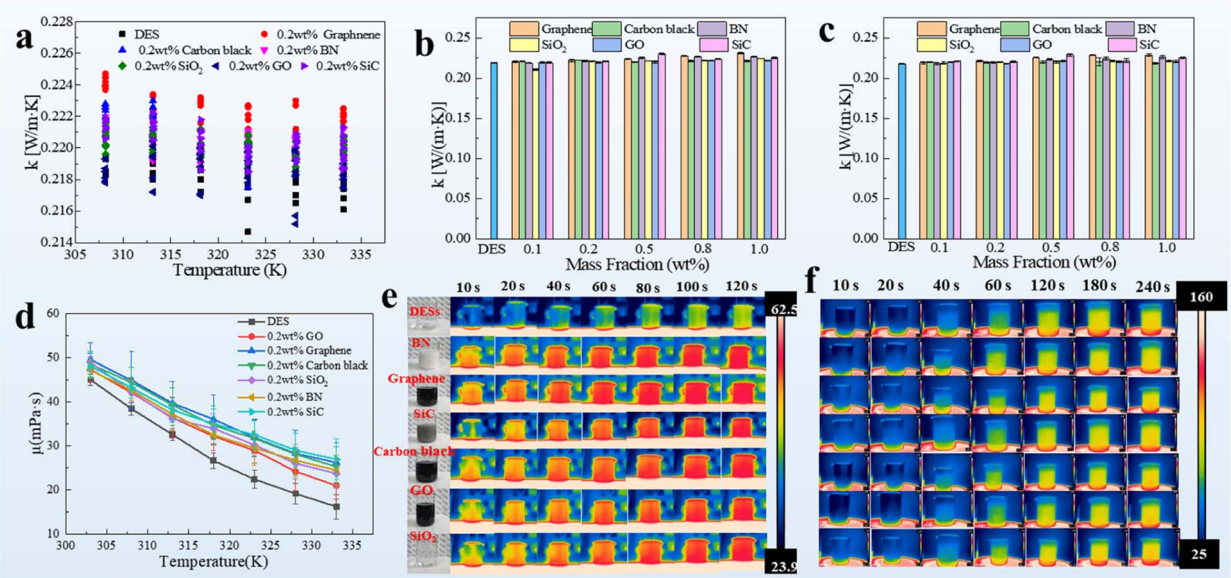


Fig. 3 Mechanistic study of cathode material recycling by determining the thermophysical properties of DES-based nanofluids. (a) *k* as a function of test temperature under a fixed mass fraction of nanofillers: *k* at (b) 30 °C and (c) 60 °C. (d) Viscosity. Dynamic images of nanofluids taken using an infrared camera being heated by an (e) 80 °C and (f) 200 °C heating plate (0.2 wt% nanofiller was used for each nanofluid).

the mass transfer in the *y*–*z* plane of the BN-filled nanofluids was more intensive than that of the other nanofluids. Owing to the fixed stirring speed, the velocity in the *x*–*z* planes was lower than that of the other samples, as proved by both cloud images and histograms (Fig. 4d and 5b). Therefore, the existence of the nanoparticles proved beneficial for the turbulence of the solution, thus enhancing the mass transfer in this specific space. Compared with the five other types of nanofillers, the BN-filled nanofluids had the most intensive mass transfer enhancement in the *y*–*z* planes, thereby clearly demonstrating their superiority in cathode material liberation.

After the average velocity of the nanofluids in a specific face was determined, more direct evidence of the distribution of cathode materials was collected. The volume fractions of the distribution of cathode materials in the *y*–*z* and *x*–*z* planes were plotted with respect to each liberation solvent (Fig. 4e and f). The addition of a nanofiller allowed the dispersion of cathode materials. However, this was not the case for GO-filled nanofluids, which showed a good agreement with the liberation data (Fig. 2b). From the cloud images, it can be seen that the BN-filled nanofluids had a clear and even distribution of cathode materials (Fig. 4e). The dynamic distribution of cathode materials was recorded through videos that were taken (ESI Videos 1 to 6†). The BN-filled nanofluids promptly dispersed the cathode materials and had the most even distribution within the same time interval. The volume fractions of cathode materials in a specific plane are presented in Fig. 5c and d. A more diluted mass concentration in the position resulted in a more even distribution of cathode materials. The BN-filled nanofluids provided the smallest cathode material mass fraction in both the *x*–*z* and *y*–*z* planes. This result was the most direct evidence demonstrating the liberation of cathode materials from spent LIBs. Therefore, although an improved heat and mass transfer effect of nanofluids was good for the liberation of cathode materials, mass transfer had a more dominant effect than heat transfer.

After knowing the heat transfer properties by means of static testing and dynamic experiments as well as the mass transfer through a CFD simulation, we can conclude that the thermal conductivity and viscosity of the seven nanofluids show slight differences in terms of static heat transfer performance. However, the dynamic monitor result really displays a difference especially in the initial 10 s and 20 s that graphene and BN nanofluids present faster heat transfer characteristics (Fig. 3e). In addition, the same phenomenon can be found in the CFD simulation results that BN filled nanofluids quite stand out and afford the rapidest velocity response, which can be recognized because graphene and BN nanofluids displayed improved mass transfer characteristic in terms of both velocity and volume fraction. These two pieces of evidence clearly proved the mechanism by which the addition of nanoparticles could enhance the heat and mass transfer of DES and lead to a significant improvement in the liberation rate consequently.

## Microstructure and chemical composition of recovered cathode materials

Complete recycling of cathode materials without damaging their microstructure and chemical composition is important as the recycling should face the downstream reuse process. Some of the commonly used methods for recovering cathode materials, such as chemical dissolution with organic solvents and mechanical–physical methods, will inevitably affect either the chemical composition or the physical structure of the cathode materials because they require harsh liberation conditions or use highly active liberation reagents. In the present study, an

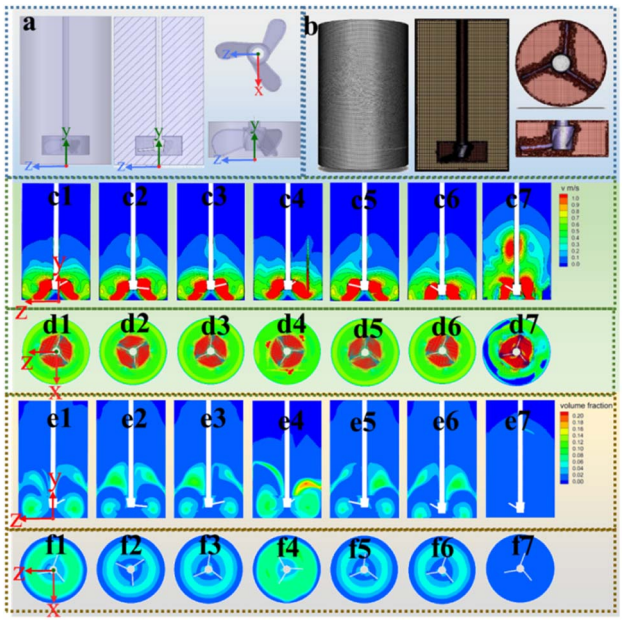


Fig. 4 Mechanistic study of the recycling of cathode materials *via* numerical CFD simulation. (a) Geometry and (b) mesh of the simulation setup. Average velocity gradient of the (c1) base solvent, (c2) graphene-nanofluids, (c3) SiC-nanofluids, (c4) GO-nanofluids, (c5) $SiO_2$-nanofluids, (c6) carbon black nanofluids and (c7) BN nanofluid-aided recycle system for cathode materials in the *y*–*z* plane. Velocity vectors of the (d1) base solvent, (d2) graphene-nanofluids, (d3) SiC-nanofluids, (d4) GO-nanofluids, (d5) $SiO_2$-nanofluids, (d6) carbon black nanofluids and (d7) BN nanofluid-aided recycle system of cathode materials in the *x*–*z* plane. Volume fraction distribution of cathode materials in (e1) base solvent, (e2) graphene-nanofluids, (e3) SiC-nanofluids, (e4) GO-nanofluids, (e5) $SiO_2$-nanofluids, (e6) carbon black nanofluids and (e7) BN nanofluids in the *y*–*z* plane. Volume fraction distribution of cathode materials in (f1) base solvent, (f2) graphene-nanofluids, (f3) SiC-nanofluids, (f4) GO-nanofluids, (f5) $SiO_2$-nanofluids, (f6) carbon black nanofluids and (f7) BN nanofluids in the *x*–*z* plane.

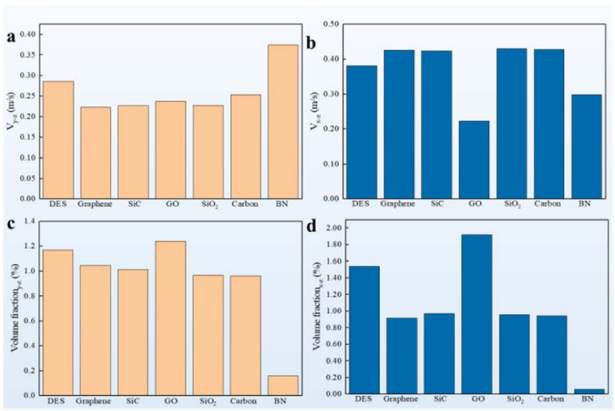


Fig. 5 Comparison of mass transfer parameters in numerical CFD simulation. (a) Average velocity gradient of the nanofluid-aided cathode material recycle system in the *y*–*z* plane. (b) Velocity vector of the nanofluid-aided cathode material recycle system in the *x*–*z* plane. Volume fraction distribution of cathode materials in the (c) *y*–*z* and (d) *x*–*z* planes.

inert solvent system, namely, EG/ChCl DESs, was used as the liberation solvent under relatively mild conditions. The cathode materials before and after the liberation treatment were analyzed *via* a scanning electron microscope (SEM), X-ray diffraction (XRD), Fourier transform infrared (FTIR) spectroscopy, and X-ray photoelectron spectroscopy (XPS). The SEM images show that the cathode material is granular both before and after the experiments. However, it is obvious that the particle arrangement of the raw material shows a piled-up morphology (Fig. 6a). And the particles are more uniformly arranged and more obviously granular after the liberation experiment (Fig. 6b). The main response within the $2\theta$ range of 10–75° was attributed to the existence of carbon, as well as Ni, Co, and Mn elements (Fig. 6c). The XRD spectra clearly show a typical response of $Li(NiCoMn)_{1/3}O_2$ before and after DES nanofluid treatment indicating that the chemical composition did not considerably change during the liberation process.[39] A similar phenomenon was observed in the FTIR spectra; however, some minor peaks, such as 1117 $cm^{-1}$, 1500 $cm^{-1}$, and 1618 $cm^{-1}$ which correspond to the C–F vibration, $CH_2$ scissoring and C=C vibration of PVDF respectively,[59] weakened or disappeared to some degree presumably because of the removal of the organic binder during the liberation process with peaks representing Ni–O, Mn–O and Co–O remaining[60](Fig. 6d). Moreover, the exact chemical state of each element was evaluated *via* XPS. Co 2p3/2 and Co 2p1/2 were observed in the XPS spectra (Fig. 6e and f). After treatment with the DES-based nanofluids, the corresponding peaks appeared in the XPS spectra that slightly changed to a high chemical shift position. This phenomenon shows a good agreement with the reported result due to the weak interaction between cobalt and the EG molecule during the liberation process.[38] The XPS spectra also revealed that the Ni element almost did not change, whereas the Mn element had a slight reduction owing to its high oxidation state[37] (Fig. 6g–j). Therefore, recycling of cathode materials using the DES-based nanofluids almost did not change both the microstructure and the chemical composition of the cathode materials. Thus, the direct downstream utilization of this recycle system is feasible, and it offers great potential for practical utilization.

## Experiments on DES recycling and metal element leaching using the DES-based nanofluids

Attempts to recycle the liberation solvent were made to verify the green metrics of the strategy for recovering cathode materials from spent LIBs. The nanofluids with 0.2 wt% BN were used as the liberation solvent, whereas pristine EG/ChCl DES was set as the control solvent (Fig. 7a–c). Errors that might be committed during the long-term experiment were prevented by shortening the reaction time to 10 h. A shortened stirring time would result in a larger difference between pristine DESs and nanofluids. Thus, strict adherence to our protocol is important. Images of DESs were taken to show changes in color for each cycle, which would indicate the leaching of metal elements in the nanofluids. Notably, the BN nanoparticles could be recycled by a simple dialysis experiment owing to their extremely small

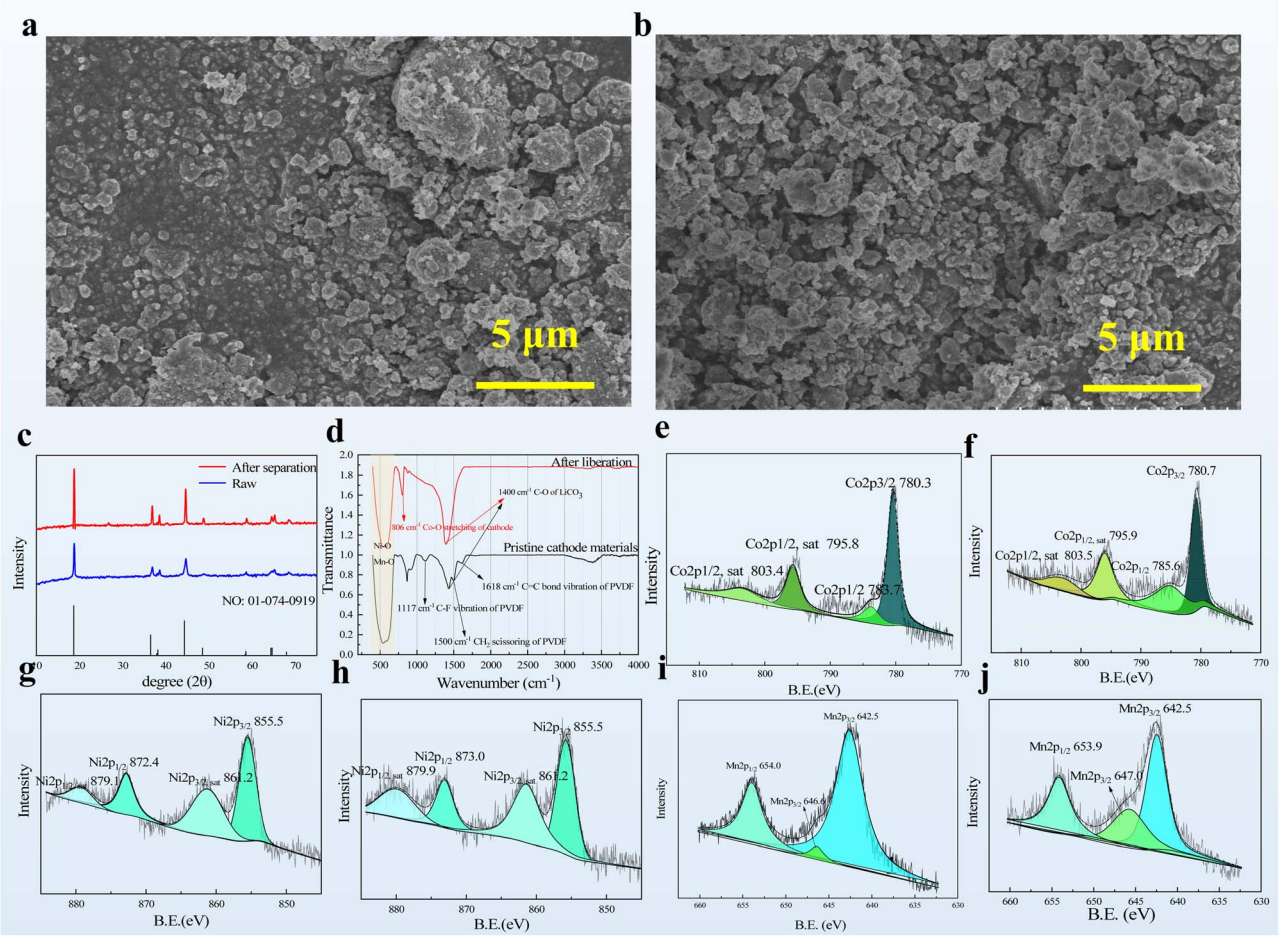


Fig. 6 Characteristics of cathode materials before and after treatment with DES-based nanofluids. SEM images (a) before and (b) after treatment with DES-based nanofluids. (c) XRD and (d) FTIR spectra before and after treatment with DES-based nanofluids. XPS analysis of Co (e) before and (f) after treatment with DES-based nanofluids. XPS analysis of Ni (g) before and (h) after treatment with DES-based nanofluids. XPS analysis of Mn (i) before and (j) after treatment with DES-based nanofluids.

size. The aluminum foil after the liberation proved the excellent liberation rate even after the fifth recycle. Indeed, the liberation rate remained over 90% even after recycling the DESs five times. Meanwhile, the chemical structure of EG/ChCl DES was analyzed *via* nuclear magnetic resonance (NMR) (Fig. 7d and e). The proton and carbon NMR spectra revealed that the chemical structure of the DESs remained stable during the recycling as the chemical shift and integration of peaks attributed to the DES molecules almost did not change. In addition, the organic binder accumulated at an amount of 3.7 ppm in the proton NMR spectra, indicating its dissolution in the DES-based nanofluids (NMR spectra of pristine PVDF can be found in ESI Note 19†). This accumulation was one of the main reasons responsible for the highly efficient liberation rate of cathode materials from LIBs. Meanwhile, some of PVDF might be decomposed in this BN/DES based nanofluid since the color change of DESs which shows a good agreement with the observation of the literature on the determination of PVDF degradation along with the broad peaks appearing at around 3.7 ppm after each recycle run.[43] Moreover, metal leaching in the DES-based nanofluids was studied because this phenomenon is associated with actual metal recycling. Compared with the traditionally used pyrometallurgy and hydrometallurgy methods, our method had obvious advantages because it requires mild reaction conditions and uses environmentally benign solvents. More importantly, real spent ternary LIBs were used in this experiment instead of commercially available cathode material alternatives. We found that the DES-based nanofluids developed herein had twofold higher leaching efficiency than pristine DES solvent systems with respect to Ni, Co, and Mn at both 120 °C and 140 °C. 100 °C was also checked and it also displays a similar trend to that of temperature at 120 °C and 140 °C (Fig. 7f).Though the DES solvent system could maintain promising liberation activity in each cycle run (Fig. 7b), leaching efficiency decreased probably owing to the accumulation of PVDF in the DES system (Table 1). Thus, our DES-based nanofluids have better heat and mass transfer performance (detailed calculation methods can be found in eqn (S1) and (S2)†). Notably, the metal concentration in the DES-based nanofluids could reach 14 300, 2990, and 3090 ppm with respect to Ni, Co, and Mn, respectively, after reacting at 140 °C for 10 h. It is worth noting that from the NMR spectra and

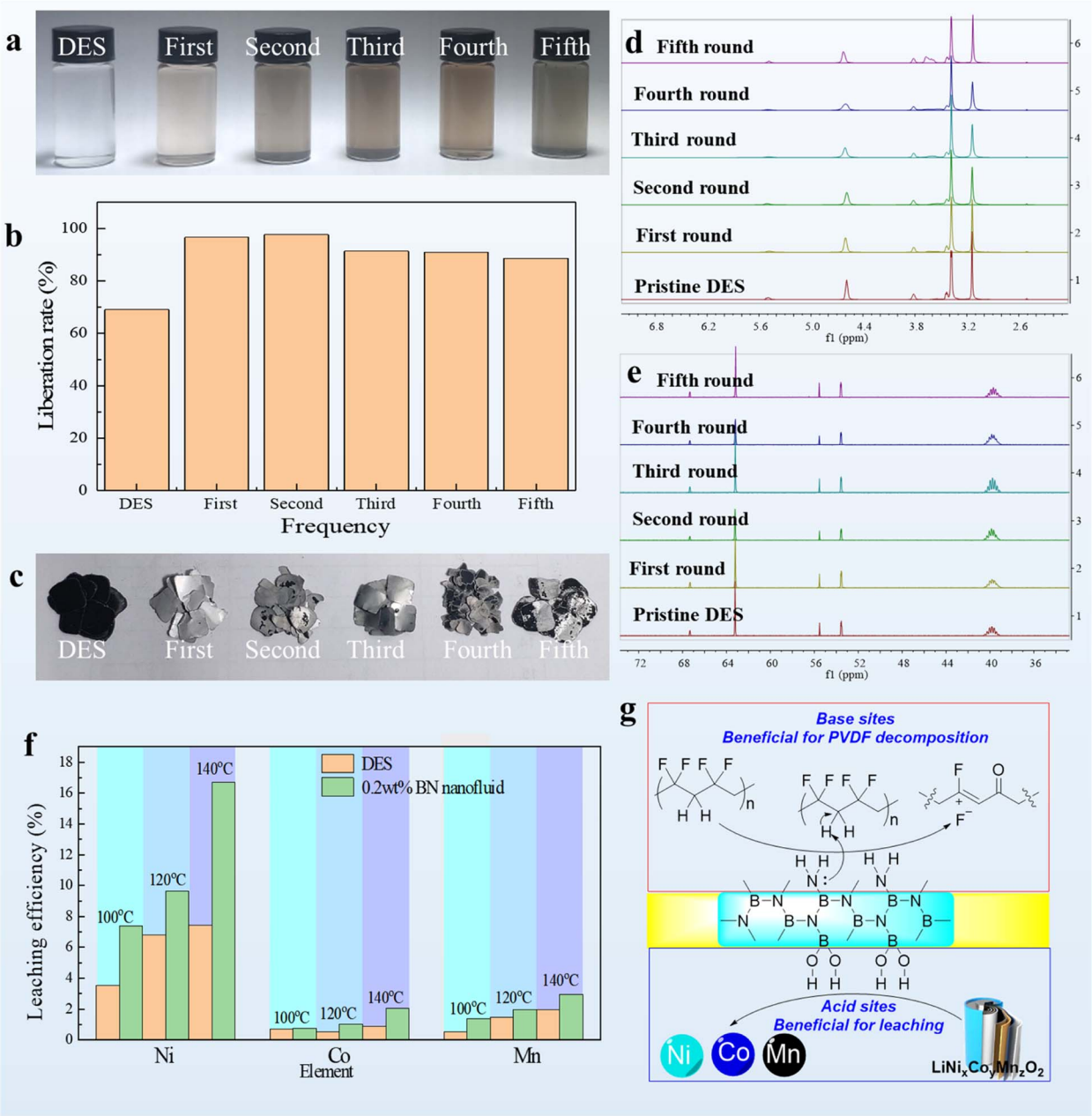


Fig. 7 Experiments on DES recycling and metal element leaching in the DES-based nanofluids. Images of (a) DESs and (c) spent cathode of LIBs after each recycle. (b) Liberation rate after each recycle. (d) Proton and (e) carbon NMR spectra of DES after each recycle. (f) Comparison of leaching efficiency between DES and 0.2 wt% BN filled nanofluids. (g) Possible mechanism for the BN enhanced cathode material liberation and leaching. For the DES recycling experiment, DES was recycled by filtration after each cathode material liberation experiment and used as a base solvent of nanofluid, with the nanofluid thereafter subjected to the downstream cathode material liberation experiment.

images of DES after each recycle, chemical reactions between each component of the recycle system can be generally excluded at 100 °C. On the other hand, to verify the reproducibility of this DES nanofluid aided cathode material liberation protocol, NMC/Li half-cells were assembled and tested for 100, 200 and 300 charge/discharge cycles respectively (see Note S20†); the batteries were then dismantled and submitted to immersion in DES based nanofluid for cathode harvesting. It is found that the cathode materials can be easily liberated from Al foil under a 100 °C stirring condition. Moreover, to further explain the reason responsible for the superior liberation and leaching efficiency over pristine EG/ChCl DESs, a possible mechanism was proposed (Fig. 7g). While BN has so far been mainly regarded as an inert material similar to graphene, it is recognized to have a variety of interesting catalytic functionalities in addition to exhibiting excellent properties as a catalyst support.[61] It was suggested that hydroxyl and amino groups were formed *via* cleavage of the B–N bond by moisture.[62] The

Table 1 Leaching efficiency of DES based nanofluids in each cycle run

| Run[a] | Leaching efficiency of Ni (%) | Leaching efficiency of Co (%) | Leaching efficiency of Mn (%) |
|---|---|---|---|
| 1 | 7.35 | 0.74 | 1.40 |
| 2 | 5.25 | 0.42 | 1.11 |
| 3 | 3.01 | 0.31 | 0.92 |
| 4 | 2.46 | 0.29 | 0.56 |
| 5 | 1.65 | 0.26 | 0.49 |

[a] The leaching process was performed at 100 °C under otherwise standard conditions.

acid and base sites could be thus formed at adjacent positions on the surface. So, the nitrogen and boron containing boron nitride are expected to function as a base and an acid simultaneously. The presence of base sites benefits the decomposition of PVDF which thus leads to an acceleration of cathode material liberation from the Al foil. Meanwhile, pseudo boric acid could have a positive effect on the leaching of $LiMO_2$ ($2LiMO_2$ + $HO–(CH_2)_2–OH + 2H^+ = 2M^{2+} + O{=}(CH_2)_2{=}O + H_2O$ (ref. 38 and 63)). Therefore, besides the positive effect in terms of heat and mass transfer which has been proved by means of studying thermophysical properties and CFD simulation, BN, a nanoparticle featuring both acid and base sites, could be used as a base to inactivate PVDF and an acid to accelerate the leaching efficiency of metal species in spent LIBs.

## Conclusions

In this work, for the first time, DES-based nanofluids were used in recovering cathode materials from spent ternary LIBs. Owing to the collaboration of DESs and nanoadditives, the liberation efficiency could reach almost 100% and the leaching efficiency with respect to Ni, Co and Mn could reach 16.7%, 2.1% and 3.0% respectively under mild conditions. A mechanistic study of the static thermal properties and dynamic observation of the nanofluids revealed that thermal conductivity enhancement plays a key role in enhancing the recycling rate of LIBs. Though the main aim of this work is the liberation of the cathode active material from spent LIBs, nano-additives in the DESs are beneficial for the metal leaching efficiency. More importantly, simulation of the recycling process *via* a CFD method showed that influence of mass transfer was greater than that of heat and mass transfer on the nanofluids. However, difficulties in the complete separation of nanoparticles from liberated cathode materials associated with the potential chemical instability of DESs at a high temperature are problems that need to be further solved. Direct utilization of nanoparticle "contaminated" spent cathode materials will probably be a feasible choice and these studies are ongoing in our laboratory.

## Author contributions

Changhui Liu: conceptualization, methodology, and writing–review and editing. Yuqi Cao: experimental data collection and writing the original draft. Tianjian Zhang, Hongqu Wu, Qingyi Liu and Wenjie Sun: carried out experiments and simulation. Zhonghao Rao and Yanlong Gu: manuscript checking.

## Conflicts of interest

There are no conflicts to declare.

## Acknowledgements

We would like to acknowledge the financial support provided by the National Natural Science Foundation of China (No. 51906252), Natural Science Foundation of Jiangsu Province (NO. BK20190632), and China Postdoctoral Science Foundation (2019M661980). The authors also thank Dr Hua Wei and Dr Rui Zhou at Advanced Analysis & Computation Center of CUMT for their assistance with SEM and XRD analysis.

## Notes and references

1 G. Harper, R. Sommerville, E. Kendrick, L. Driscoll, P. Slater, R. Stolkin, A. Walton, P. Christensen, O. Heidrich, S. Lambert, A. Abbott, K. S. Ryder, L. Gaines and P. Anderson, *Nature*, 2019, **575**, 75–86.
2 H. Jin, S. Xin, C. Chuang, W. Li, H. Wang, J. Zhu, H. Xie, T. Zhang, Y. Wan, Z. Qi, W. Yan, Y.-R. Lu, T.-S. Chan, X. Wu, J. B. Goodenough, H. Ji and X. Duan, *Science*, 2020, **370**, 192–197.
3 K. Marker, C. Xu and C. P. Grey, *J. Am. Chem. Soc.*, 2020, **142**, 17447–17456.
4 X. Lai, Y. Huang, H. Gu, C. Deng, X. Han, X. Feng and Y. Zheng, *Energy Storage Mater.*, 2021, **40**, 96–123.
5 H. Lv, H. Huang, C. Huang, Q. Gao, Z. Yang and W. Zhang, *Appl. Catal., B*, 2021, **283**, 119634.
6 A. R. Dehghani-Sanij, E. Tharumalingam, M. B. Dusseault and R. Fraser, *Renewable Sustainable Energy Rev.*, 2019, **104**, 192–208.
7 B. Jang, M. Park, O. B. Chae, S. Park, Y. Kim, S. M. Oh, Y. Piao and T. Hyeon, *J. Am. Chem. Soc.*, 2012, **134**, 15010–15015.
8 C. Lei, I. Aldous, J. M. Hartley, D. L. Thompson, S. Scott, R. Hanson, P. A. Anderson, E. Kendrick, R. Sommerville, K. S. Ryder and A. P. Abbott, *Green Chem.*, 2021, **23**, 4710–4715.
9 J. Zhao, X. Qu, J. Qu, B. Zhang, Z. Ning, H. Xie, X. Zhou, Q. Song, P. Xing and H. Yin, *J. Hazard. Mater.*, 2019, **379**, 120817.
10 L. Zhuang, C. Sun, T. Zhou, H. Li and A. Dai, *Waste Manag.*, 2019, **85**, 175–185.
11 J. Li, M. Yang, Z. Huang, B. Zhao, G. Zhang, S. Li, Y. Cui, Z. Dong and H. Liu, *Chem. Eng. J.*, 2021, **417**, 129249.
12 C. Xu, W. Xiang, Z. Wu, L. Qiu, Y. Ming, W. Yang, L. Yue, J. Zhang, B. Zhong, X. Guo, G. Wang and Y. Liu, *Chem. Eng. J.*, 2021, **403**, 126314.
13 D. J. Garole, R. Hossain, V. J. Garole, V. Sahajwalla, J. Nerkar and D. P. Dubal, *Chemsuschem*, 2020, **13**, 3079–3100.
14 J. Li, Y. Lu, T. Yang, D. Ge, D. L. Wood III and Z. Li, *Iscience*, 2020, **23**, 101081.
15 B. Gault and J. D. Poplawsky, *Nat. Commun.*, 2021, **12**, 101081.

16 J. Moon, H. C. Lee, H. Jung, S. Wakita, S. Cho, J. Yoon, J. Lee, A. Ueda, B. Choi, S. Lee, K. Ito, Y. Kubo, A. C. Lim, J. G. Seo, J. Yoo, S. Lee, Y. Ham, W. Baek, Y.-G. Ryu and I. T. Han, *Nat. Commun.*, 2021, **12**, 2714.
17 H. Zhang, C. Li, G. G. Eshetu, S. Laruelle, S. Grugeon, K. Zaghib, C. Julien, A. Mauger, D. Guyomard, T. Rojo, N. Gisbert-Trejo, S. Passerini, X. Huang, Z. Zhou, P. Johansson and M. Forsyth, *Angew. Chem., Int. Ed.*, 2020, **59**, 534–538.
18 H. Gan, R. Wang, J. Wu, H. Chen, R. Li and H. Liu, *ACS Appl. Mater. Interfaces*, 2021, **13**, 37162–37171.
19 Y. Liu, B. Yang, X. Dong, Y. Wang and Y. Xia, *Angew. Chem., Int. Ed.*, 2017, **56**, 16606–16610.
20 X. Zhang, L. Li, E. Fan, Q. Xue, Y. Bian, F. Wu and R. Chen, *Chem. Soc. Rev.*, 2018, **47**, 7239–7302.
21 C. P. Grey and D. S. Hall, *Nat. Commun.*, 2020, **11**, 6279.
22 M. Li and J. Lu, *Science*, 2020, **367**, 979–980.
23 Y. Jin, T. Zhang and M. Zhang, *Adv. Energy Mater.*, 2022, **12**, 2201526.
24 R. Morina, D. Callegari, D. Merli, G. Alberti, P. Mustarelli and E. Quartarone, *ChemSusChem*, 2022, **15**, e202102080.
25 K. Du, E. H. Ang, X. Wu and Y. Liu, Progresses in Sustainable Recycling Technology of Spent Lithium-Ion Batteries, *Energy Environ. Mater.*, 2022, **5**, 1012–1036.
26 B. Makuza, Q. Tian, X. Guo, K. Chattopadhyay and D. Yu, *J. Power Sources*, 2021, **491**, 229622.
27 G. P. Nayaka, K. V. Pai, G. Santhosh and J. Manjanna, *Hydrometallurgy*, 2016, **161**, 54–57.
28 R. Golmohammadzadeh, F. Rashchi and E. Vahidi, *Waste Manag.*, 2017, **64**, 244–254.
29 Y. Xu, D. Song, L. Li, C. An, Y. Wang, L. Jiao and H. Yuan, *J. Power Sources*, 2014, **252**, 286–291.
30 A. Porvali, M. Aaltonen, S. Ojanen, O. Velazquez-Martinez, E. Eronen, F. Liu, B. P. Wilson, R. Serna-Guerrero and M. Lundstrom, *Resour., Conserv. Recycl.*, 2019, **142**, 257–266.
31 J. R. Almeida, M. N. Moura, R. V. Barrada, E. M. Sartori Barbieri, M. T. Weitzel Dias Carneiro, S. A. Duarte Ferreira, M. d. F. Fontes Lelis, M. B. Jose Geraldo de Freitas and G. P. Brandao, *Sci. Total Environ.*, 2019, **685**, 589–595.
32 G. Zhang, X. Yuan, Y. He, H. Wang, W. Xie and T. Zhang, *Waste Manag.*, 2020, **115**, 113–120.
33 Y. Chen, Y. Lu, Z. Liu, L. Zhou, Z. Li, J. Jiang, L. Wei, P. Ren and T. Mu, *ACS Sustainable Chem. Eng.*, 2020, **8**, 11713–11720.
34 M. Jesus Roldan-Ruiz, M. Luisa Ferrer, M. Concepcion Gutierrez and F. del Monte, *ACS Sustainable Chem. Eng.*, 2020, **8**, 5437–5445.
35 V. Agieienko and R. Buchner, *Phys. Chem. Chem. Phys.*, 2022, **24**, 5265–5268.
36 M. K. Tran, M.-T. F. Rodrigues, K. Kato, G. Babu and P. M. Ajayan, *Nat. Energy*, 2019, **4**, 339–345.
37 S. Wang, Z. Zhang, Z. Lu and Z. Xu, *Green Chem.*, 2020, **22**, 4473–4482.
38 S. Tang, M. Zhang and M. Guo, *ACS Sustainable Chem. Eng.*, 2022, **10**, 975–985.
39 S. Tang, J. Feng, R. Su, M. Zhang and M. Guo, *ACS Sustainable Chem. Eng.*, 2022, **10**, 8423–8432.
40 X. Chang, M. Fan, C. F. Gu, W. H. He, Q. Meng, L. J. Wan and Y. G. Guo, *Angew. Chem., Int. Ed. Engl.*, 2022, **61**, e202202558.
41 P. G. Schiavi, P. Altimari, M. Branchi, R. Zanoni, G. Simonetti, M. A. Navarra and F. Pagnanelli, *Chem. Eng. J.*, 2021, **417**, 129249.
42 D. L. Thompson, I. M. Pateli, C. Lei, A. Jarvis, A. P. Abbott and J. M. Hartley, *Green Chem.*, 2022, **24**, 4877–4886.
43 K. Jafari, M. H. Fatemi and P. Estellé, *J. Mol. Liq.*, 2021, **321**, 114752.
44 C. Hanisch, T. Loellhoeffel, J. Diekmann, K. J. Markley, W. Haselrieder and A. Kwade, *J. Cleaner Prod.*, 2015, **108**, 301–311.
45 C. Lei, I. Aldous, J. M. Hartley, D. L. Thompson, S. Scott, R. Hanson, P. A. Anderson, E. Kendrick, R. Sommerville, K. S. Ryder and A. P. Abbott, *Green Chem.*, 2021, **23**, 4710–4715.
46 G. Zhang, Y. He, Y. Feng, H. Wang, T. Zhang, W. Xie and X. Zhu, *J. Cleaner Prod.*, 2018, **199**, 62–68.
47 M. Wang, Q. Tan, L. Liu and J. Li, *J. Hazard. Mater.*, 2019, **380**, 120846.
48 H. Ben, J. Belghaieb and N. Hajji, *Therm. Sci.*, 2018, **22**, 3107–3120.
49 T. Ma, Z. Guo, M. Lin and Q. Wang, *Renewable Sustainable Energy Rev.*, 2021, **138**, 110494.
50 J. Kim and H. Park, *J. Energy Storage*, 2021, **38**, 102529.
51 N. Oger, Y. F. Lin, C. Labrugère, E. Le Grognec, F. Rataboul and F.-X. Felpin, *Carbon*, 2016, **96**, 342–350.
52 H. Q. Liu, K. Y. Sun, X. Y. Shi, H. N. Yang, H. S. Dong, Y. Kou, P. Das, Z. S. Wu and Q. Shi, *Energy Storage Mater.*, 2021, **42**, 845–870.
53 Q. Zhang, K. De Oliveira Vigier, S. Royer and F. Jérôme, *Chem. Soc. Rev.*, 2012, **41**, 7108–7146.
54 C. Liu, H. Fang, X. Liu, B. Xu and Z. Rao, *ACS Sustainable Chem. Eng.*, 2019, **7**, 20159–20169.
55 C. Liu, H. Fang, Y. Qiao, J. Zhao and Z. Rao, *Int. J. Heat Mass Transfer*, 2019, **138**, 690–698.
56 C. Liu, P. Jiang, Y. Huo, T. Zhang and Z. Rao, *Heat Mass Transfer*, 2021, DOI: **10.1007/s00231-021-03030-z**.
57 T. Elperin and A. Fominykh, *Chem. Eng. Sci.*, 2001, **56**, 3065–3074.
58 A. I. Shallan, Y. Tavares, M. Navvab Kashani, M. C. Breadmore and C. Priest, *Angew. Chem., Int. Ed.*, 2020, **60**, 2654–2657.
59 X. Zhao, L. Song, J. Fu, P. Tang and F. Liu, *J. Hazard. Mater.*, 2011, **189**, 732–740.
60 Q. Wu, Y. Yin, S. Sun, X. Zhang, N. Wan and Y. Bai, *Electrochim. Acta*, 2015, **158**, 73–80.
61 S. Nakamura, A. Takagaki, M. Watanabe, K. Yamada, M. Yoshida and T. Ishihara, *ChemCatChem*, 2020, **12**, 6033–6039.
62 A. Takagaki, *Catal. Today*, 2020, **352**, 279–286.
63 S. Tang, J. Feng, R. Su, M. Zhang and M. Guo, *ACS Sustainable Chem. Eng.*, 2022, **10**, 8423–8432.